Ultrathin Carbon Molecular Sieve Membrane for Propylene/Propane Separation

Xiaoli Ma and Y. S. Lin
School for Engineering of Matter, Transport and Energy, Arizona State University, Tempe, AZ 85287

Xiaotong Wei and Jay Kniep
Membrane Technology and Research, Inc., Newark, CA 94560

DOI 10.1002/aic.15005
Published online August 31, 2015 in Wiley Online Library (wileyonlinelibrary.com)

Ultrathin (down to 300 nm), high quality carbon molecular sieve (CMS) membranes were synthesized on mesoporous γ-alumina support by pyrolysis of defect free polymer films. The effect of membrane thickness on the micropore structure and gas transport properties of CMS membranes was studied with the feed of He/N_2 and C_3H_6/C_3H_8 mixtures. Gas permeance increases with constant selectivity as the membrane thickness decreases to 520 nm. The 520-nm CMS membrane exhibits C_3H_6/C_3H_8 mixture selectivity of ∼31 and C_3H_6 permeance of $\sim 1.0 \times 10^{-8}$ mol m^{-2} s^{-1} Pa^{-1}. Both C_3H_8 permeance and He/N_2 selectivity increase, but the permeance of He, N_2, and C_3H_6 and the selectivity of C_3H_6/C_3H_8 decrease with further decrease in membrane thickness from 520 to 300 nm. These results can be explained by the thickness-dependent chain mobility of the polymer film which yields thinner final CMS membranes with reduction in pore size and possible closure of C_3H_6-accessible micropores. © 2015 American Institute of Chemical Engineers *AIChE J*, 62: 491–499, 2016
Keywords: carbon molecular sieve membrane, γ-alumina, propylene/propane separation, ultrathin, glass transition temperature

Introduction

Carbon molecular sieve (CMS) membranes are formed by pyrolysis/carbonization of polymeric precursor membranes under controlled vacuum or inert atmosphere.[1–3] The slit-like micropore structure of CMS membrane can be finely tuned through the selection of polymer precursors and varying pyrolysis conditions to offer strong molecular sieving effect toward gas pairings, such as H_2/CO_2, O_2/N_2, CO_2/N_2, CO_2/CH_4, and C_3H_6/C_3H_8, for which conventional polymeric membranes do not offer great selectivities.[4–7] Among them, using CMS for the separation of C_3H_6 and C_3H_8 is even more promising, because of the high product value and high energy-intensity of the existing separation technology.[8–10] Several research groups have successfully fabricated CMS membranes with superior C_3H_6/C_3H_8 separation performance exceeding the upper bound curve between permeability and selectivity for conventional polymeric membranes,[11–14] making CMS membrane one of the most promising candidates for C_3H_6/C_3H_8 separation.

The membrane performance determines the productivity of the membrane system.[15] For a given membrane material, permeance enhancement can be achieved by lowering the thickness of the selective layer. However, it is challenging to fabricate thin, high quality membranes without compromising the membrane selectivity. So far, researchers have prepared the CMS membranes in two different forms in an effort to achieve high permeances: asymmetric hollow fiber and thin-film composite membranes using inorganic substrates.

Hollow fiber membranes offer advantages of high packing density than thin-film composite membranes. Okamoto et al.[12] prepared hollow fiber CMS membranes with a selective layer of approximately 200 nm, and the membrane exhibited a high C_3H_6 permeance of 8.7×10^{-9} mol m^{-2} s^{-1} Pa^{-1} (26 GPU) and C_3H_6/C_3H_8 selectivity of 11 at 35°C. The relatively low selectivity suggested the existence of nonselective defects in the membrane. Recently, Koros and coworkers[13] found that the porous substructure of Matrimid hollow fiber membrane densifies during pyrolysis, resulting in an increased effective separation layer thickness. In another study, Koros and coworkers reported a pre-pyrolysis treatment method using a sol-gel crosslinking reaction to induce vinyl crosslinked silica on precursor fiber walls to restrict the morphology collapse.[14] The treated membranes possess an apparent membrane skin thickness of 5–6 μm for Matrimid derived membrane and 3–4 μm for 6FDA derived membrane, 5–6 fold thinner than the CMS membranes from untreated precursors.[14]

Thin-film composite CMS membranes can be prepared by coating the polymer precursor film on ceramic support followed by pyrolysis. The resultant CMS membrane layer has a symmetric pore structure with the thickness essentially determined by the thickness of the coated polymer layer. Most composite CMS membranes reported in literature have an effective membrane thickness larger than 2 μm, because a certain membrane layer is required to cover the surface defects and the macropores of inorganic substrate.[16–19] This is especially important in fabricating CMS membrane with high selectivity

Correspondence concerning this article should be addressed to Y. S. Lin at jerry.lin@asu.edu.

Table 1. Preparation Conditions of γ-Alumina Supported Polymer Membranes

Polymer Membrane	Polymer Concentration (wt %)	Dip-Coating Time (s)
P-2-60	2	60
P-2-30	2	30
P-2-15	2	15
P-1-15	1	15
P-0.5-15	0.5	15
P-0.2-15	0.2	15

for separation of propylene/propane gas pairs of very close molecular sizes. Hayashi et al.[18] fabricated a BPDA-pp′ODA polyimide derived CMS membrane on the outer surface of a porous alumina tubular support (average pore size, 140 nm) by repeating the coating/carbonization two or three times. The prepared membrane showed a high C_3H_6/C_3H_8 mixture selectivity of 46 but a low C_3H_6 permeance of 7.9×10^{-10} mol m^{-2} s^{-1} Pa^{-1} (2.4 GPU) due to the large membrane thickness of 5–6 μm. Single-time dip-coating was used by Yamamoto et al.[19] to form the polymer precursor film on alumina support before pyrolysis. However, their membranes are still of 4–6 μm in thickness and only offered unattractive C_3H_6 permeances lower than 3.0×10^{-9} mol m^{-2} s^{-1} Pa^{-1}.

Despite these efforts on synthesis of the thin CMS membranes discussed above, there was essentially no study reported on synthesis and transport properties of high quality CMS membrane with submicron thickness. It has been reported that the film thickness affects weight loss, amounts of evolved compounds and the degree of graphitization of polyimide-derived carbon films.[20,21] But the influence of thickness, especially when it is down to the submicron range, on the properties of microporous carbon membranes is still unknown. Our group recently demonstrated that high quality CMS membrane can be synthesized on mesoporous γ-alumina, rather than on the commonly used macroporous support.[22] This advancement in CMS membranes enabled us to synthesize CMS membranes of various thicknesses down to submicron range. This article will report synthesis of ultrathin CMS membranes on γ-alumina substrates with high C_3H_6 gas permeance for C_3H_6/C_3H_8 separation, and study of the effect of membrane thickness on the structure and gas transport properties of CMS membranes. The main objective of this work is to understand the synthesis-structure-gas permeation property relationship for thin CMS membrane based on the gas permeation and separation results of polymer and CMS membranes of different thicknesses.

Experimental

Preparation of polymer membranes

Ceramic supports with an asymmetric structure consisting of a γ-alumina top layer and α-alumina substrate were used as the supports for membrane preparation. The α-alumina supports with a porosity of ~45% and an average pore diameter of ~200 nm were prepared by sintering α-alumina disk at 1150°C for 30 h. One side of the α-alumina support was polished with sandpaper (#500, #800, and #1200). The boehmite sol was prepared following previously reported procedures,[23,24] and then coated onto the polished side of α-alumina support. The whole support was then calcined at 550°C for 3 h with a heating and cooling rate of 0.5°C min^{-1}. If necessary, the coating and calcination was repeated to get a final good quality γ-alumina layer.

The polymer precursor used in this work is a proprietary 6FDA-based polyimide polymer (molecular weight >30,000) provided by Membrane Technology and Research. The precursor was dissolved in acetone to prepare polymer coating solutions with different concentrations from 1 to 0.2 wt %. The polymer membranes were formed on the surface of γ-alumina support by dip-coating method. The dip-coating time was varied from 15 to 30 s and 60 s. Different polymer concentration and different dip-coating time were used to give polymer membranes with different thicknesses. Detailed preparation conditions of polymer membranes were listed in Table 1. The polymer membranes were named in the form of P-concentration of polymer solution-dip coating time. These supported polymer membranes were first dried at room temperature for 3 h, then at 100°C for 12 h, and finally annealed at 140°C in air for 5 h.

Preparation of CMS membranes

CMS membranes with different thicknesses were formed by pyrolysis of the supported polymer membranes under ultra high purity (UHP) argon gas environment. The oxygen level in the pyrolysis gas is crucial to the quality of CMS membranes prepared by this method. Depending on the concentrations, the oxygen could damage the membrane due to excessive decomposition of the polymer film,[25] or improve the membrane performance through oxygen doping in the micropores.[26] To avoid any effects from oxygen and to maintain the same pyrolysis conditions for all membranes, an additional oxygen removal step using copper-based catalyst (Research Catalysts) as "oxygen getter" was applied in this work.

Figure 1 shows the schematic setup for the oxygen removal assisted pyrolysis process. The copper catalysts were closely packed inside the left tubular furnace to form a fixed-bed reactor. The catalysts, which came as copper oxides, were first activated by reduction of the copper oxides to metallic copper using a reducing 2% H_2/Ar mixture at a flow rate of 100 mL min^{-1} at 175°C for 24 h. After the activation, the polymer membranes were placed inside the furnace on the right side and UHP Ar gas at a flow rate of 100 mL min^{-1} was used for pyrolysis. The copper catalyst reacted with the oxygen impurities existing in the UHP Ar to form copper oxide. As a result, an almost oxygen free environment was created for the downstream pyrolysis process. The pyrolysis was typically conducted at 550°C for 2 h with a heating and cooling rate of 4°C min^{-1}. The pyrolysis conditions including the final pyrolysis temperature and thermal soak time were varied for the ultra thin CMS membrane. All the CMS membranes prepared were stored in UHP Ar atmosphere before gas permeation and separation test, to avoid any water or oxygen adsorption on membrane.[27]

Membrane characterization and single gas permeation measurements

The surface morphology and cross-section of the polymer membranes and CMS membranes were characterized by scanning electron microscopy (SEM, Philips, XL 30) at an accelerating voltage of 20 kV. The thicknesses were determined from the cross-section SEM images of these membranes. Fourier transform infrared spectroscopy (FTIR) spectra for the CMS membranes were collected by a Nicolet 4700 FT-IR spectrometer.

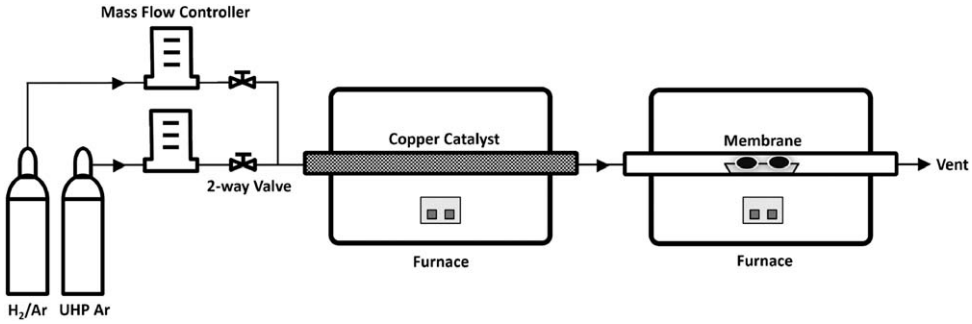

Figure 1. Schematic setup for the oxygen removal assisted pyrolysis of CMS membrane.

The He and N_2 single gas permeances through the polymer membranes were measured by a previously reported steady-state method at room temperature,[28] with a feed pressure of 45 psi. The He/N_2 perm-selectivity was calculated based on the ratio of He and N_2 single gas permeance, and was used to examine the membrane quality. In the physical aging test of polymer membranes, the permeances of He and N_2 were monitored over 72 h. To facilitate comparison of the rate of physical aging, the He, N_2 permeances, and He/N_2 perm-selectivity were normalized by the corresponding initial values of the membranes.

Mixture separation measurement

The C_3H_6/C_3H_8 mixture separation performance of the CMS membranes was measured using a previously reported cross-flow setup.[22,29] The feed side was a 50%/50% C_3H_6/C_3H_8 mixture at a total flow rate of 50 mL min^{-1}, and N_2 at a flow rate of 50 mL min^{-1} was used as sweeping gas on the permeate side. The feed pressure was maintained at 45 psi (310 kPa) by a needle valve on the retentate line. The gas flow rate on the permeate side was measured by a bubble flow meter. The gas composition on the permeate side was measured by gas chromatography (SRI Instruments, SRI 8610C) equipped with a flame ionization detector and a $6' \times 1/8''$ silica gel packed column, using He as carrier gas. All the measurements were conducted at room temperature.

The He/N_2 mixture separation properties of CMS membranes were measured with a 50%/50% He/N_2 mixture using the same cross-flow setup. Ar gas with a flow rate of 50 mL min^{-1} was used as sweeping gas. The gas composition on the permeate side was measured by a GC (Agilent 6890N) with a thermal conductivity detector detector and an AllTech HayeSep DB 100/120 column. All the gas permeation measurements were conducted three times to determine the average values for permeance and selectivity. The errors for the triplicate measurements are in the range of 3–10%.

Results and Discussion

Polymer membranes with different thicknesses

The mesoporous γ-alumina supports prepared in this work have a pore size of ~3 nm and a surface roughness of ~4 nm, and are all of good quality with the gas transport showing Knudsen diffusion behavior. Coating a γ-alumina layer of several microns thick only causes a 20–30% reduction in the gas permeance of α-alumina support, ensuring negligible gas transport resistance through the support as compared with the polymer or CMS membrane.

Figures 2 and 3 show the He and N_2 gas permeation properties of the membranes after the supports were coated with the polymer precursors at different conditions. For membranes coated with the same polymer solution (P-2-60, P-2-30, P-2-15) shown in Figure 2, with the decrease of dip-coating time, the permeance of both He and N_2 increases while the perm-selectivity stays essentially constant. The increase in gas permeance is more obvious for the membranes prepared with a more diluted polymer solution. As shown in Figure 3, at a fixed dip-coating time of 15 s, the permeance increases by about eight times as the concentration of the dip-coating

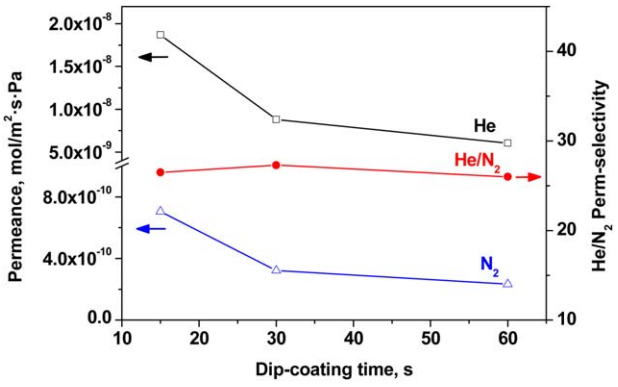

Figure 2. Effect of dip coating time on the He and N_2 permeation through polymer membranes.

[Color figure can be viewed in the online issue, which is available at wileyonlinelibrary.com.]

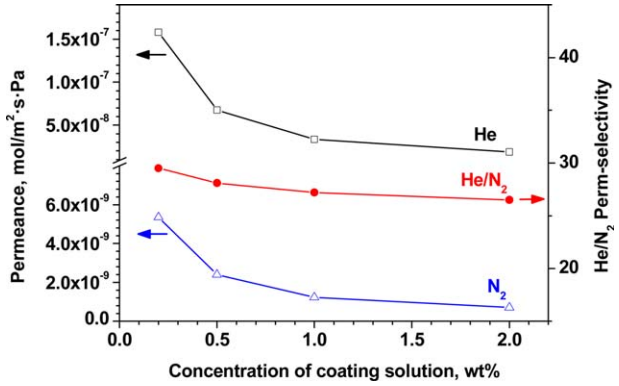

Figure 3. Effect of the concentration of polymer coating solution on the He and N_2 permeation through polymer membranes.

[Color figure can be viewed in the online issue, which is available at wileyonlinelibrary.com.]

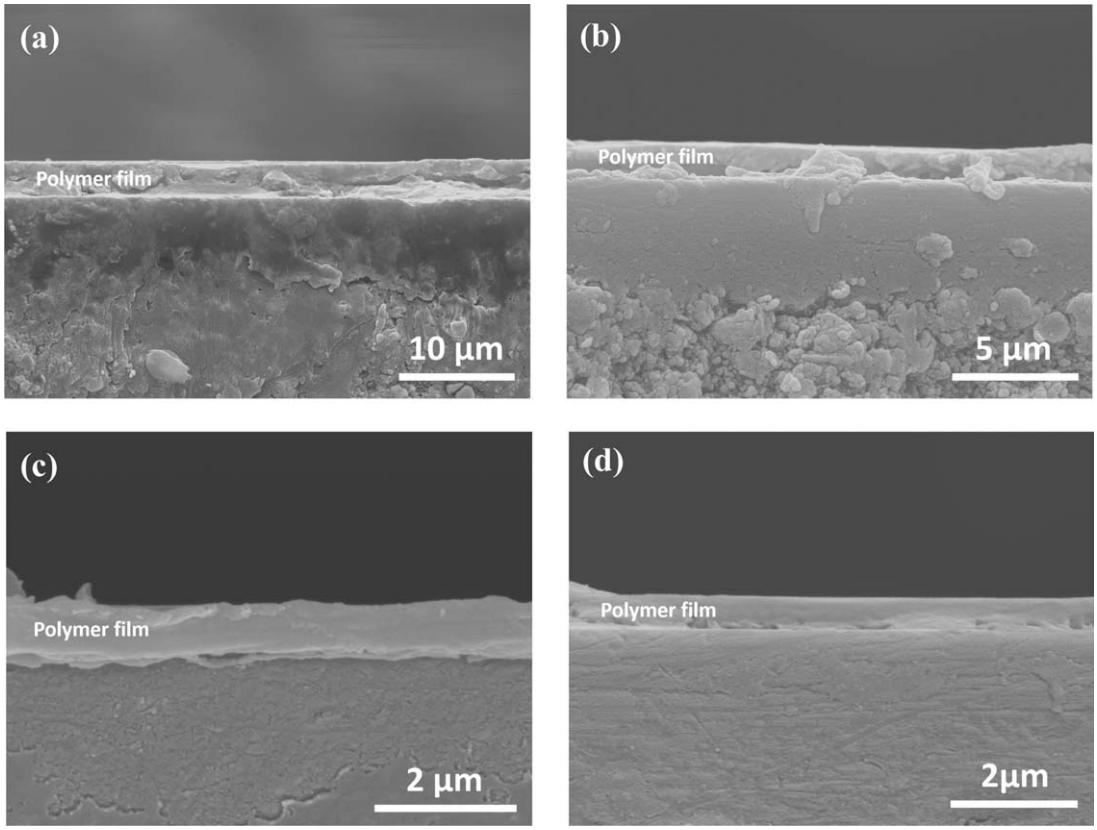

Figure 4. Cross-section SEM images of γ-alumina supported polymer membranes with different thicknesses: (a) P-2-15, (b) P-1-15, (c) P-0.5-15, and (d) P-0.2-15.

solution decreases from 2 to 0.2 wt %. These membranes all show good He/N_2 perm-selectivities of above 26, suggesting the absence of any large defects. Overall, higher gas permeance results from lowering thickness of the polymer layer, which can be achieved by shortening the dip-coating time or lowering the concentration of the coating solutions. It should be noted that membrane P-0.2-15 shows a slightly higher He/N_2 perm-selectivity than others. This could be because the polymer chains are more uniformly dispersed and less tangled together in the more diluted solution, which consequently leads to a more closely packed polymer chains in the polymer film coated on the support. Another possible reason is the faster physical aging for the thinner polymer membrane, as will be discussed later.

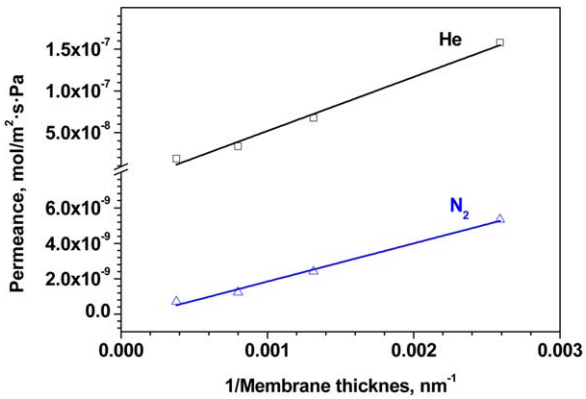

Figure 5. He and N_2 permeances of the polymer membranes as a function of the reciprocal of membrane thickness.

[Color figure can be viewed in the online issue, which is available at wileyonlinelibrary.com.]

To verify the infiltration of polymers into the support pores, the cross-section of the membranes were characterized by SEM and the images are shown in Figure 4. The SEM images confirm the decrease of membrane thickness with lowering the concentration of coating solutions. Although a distinct boundary can be found between the polymer film and the γ-alumina layer, the infiltration of polymers is difficult to be observed under the used magnifications. With the thickness information obtained from the SEM cross-section images, the He and N_2 gas permeances were plotted as a function of the reciprocal of the thickness, as is shown in Figure 5. A clear linear relationship between the permeance and the reciprocal of membrane thickness was observed. This indicates no penetration of polymer chains into the support pores even under the conditions of using very diluted polymer solutions. These high quality polymer membranes were pyrolyzed to form CMS membranes with different thicknesses.

CMS membranes with different thicknesses

Figure 6 shows the cross-section SEM images of the CMS membranes with different thicknesses after pyrolysis at 550°C for 2 h. The three-layer structure consisting of carbon layer, γ-alumina layer, and α-alumina support are clearly shown in the SEM images. These membranes are of high integrity with no macroscopic defects found on the surface SEM images (not shown here). The SF_6 (0.55 nm) permeance for the membranes is smaller than 1×10^{-11} mol m^{-2} s^{-1} Pa^{-1}, further indicating the presence of limited defects. The FTIR spectra of the CMS membranes with different thicknesses are shown in

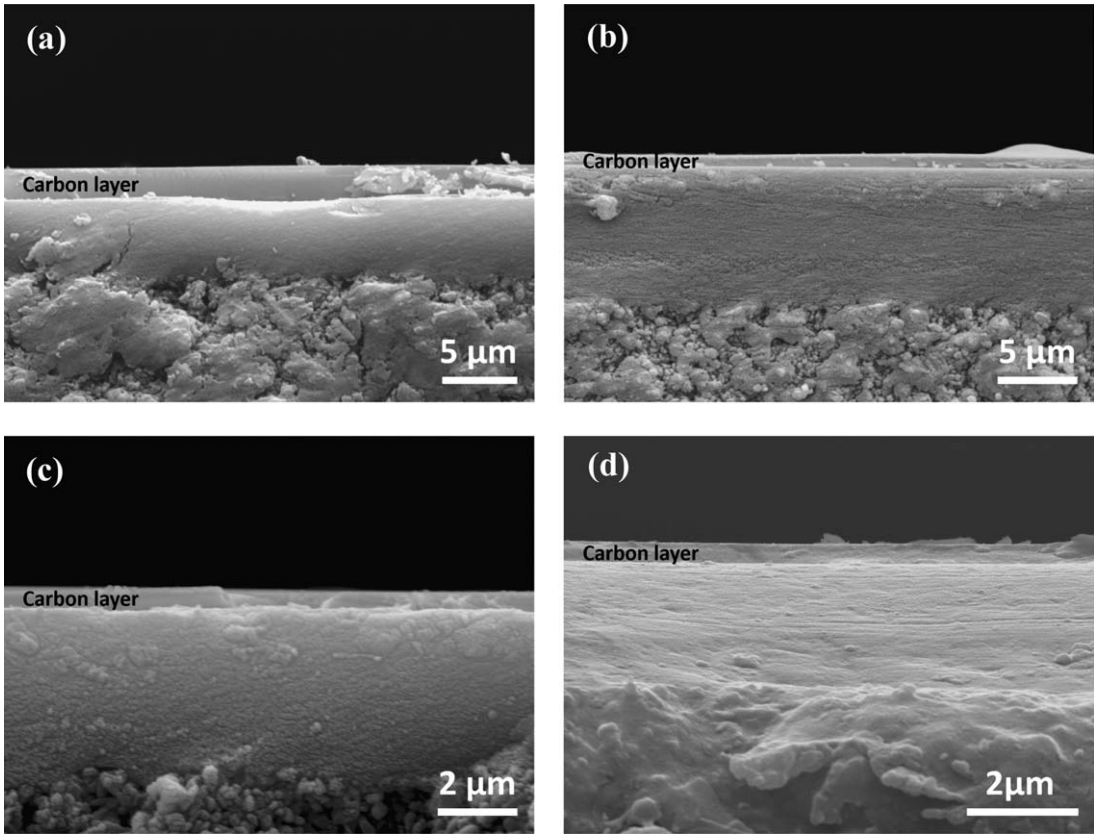

Figure 6. Cross-section SEM images of γ-alumina supported CMS membranes with different thicknesses: (a) 2.1 μm, (b) 850 nm, (c) 520 nm, and (d) 300 nm.

Figure 7. All these membranes exhibit a relatively strong band at 1605 cm^{-1} ascribed to C═C bond, and tiny bands at 1723 and 1350 cm^{-1} which come from the residual oxygen and nitrogen heteroatoms on the membrane surface. The similar spectra observed for these membranes suggest no change of the surface functional groups with the change of membrane thickness.

Figure 8 shows the mixed-gas permeances and selectivity of He and N_2 for membranes with different thicknesses. When the carbon layer thickness decreases from 2100 to 520 nm, both He and N_2 permeances increase accordingly with a slight decrease in He/N_2 selectivity. However, it is interesting to note that further reducing the thickness from 520 to 300 nm results in a decrease in the gas permeances but an increase in He/N_2 selectivity. This appears to indicate a reduction in the effective pore size when the carbon layer thickness is reduced beyond 520 nm. Figure 9 shows the C_3H_6/C_3H_8 separation performance as a function of membrane thickness. Similar to the trend for He/N_2 system, the C_3H_6 permeance is improved without compromising the selectivity by reducing the membrane thickness to 520 nm. However, the 300 nm membrane shows a dramatically decreased C_3H_6/C_3H_8 selectivity, due to

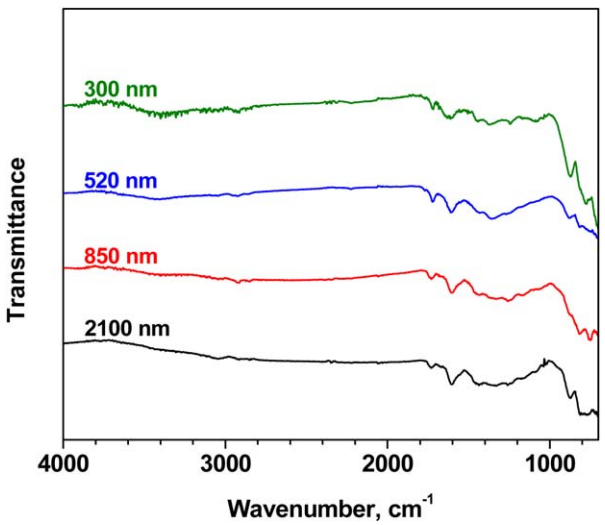

Figure 7. FTIR spectra of CMS membranes with different membrane thicknesses.

[Color figure can be viewed in the online issue, which is available at wileyonlinelibrary.com.]

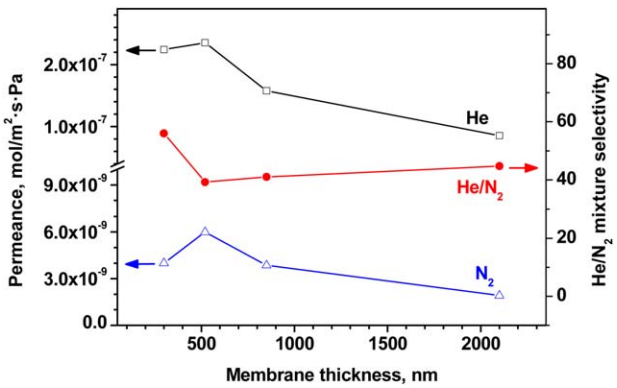

Figure 8. He, N_2 permeances and He/N_2 mixture selectivity of CMS membranes as a function of membrane thickness.

[Color figure can be viewed in the online issue, which is available at wileyonlinelibrary.com.]

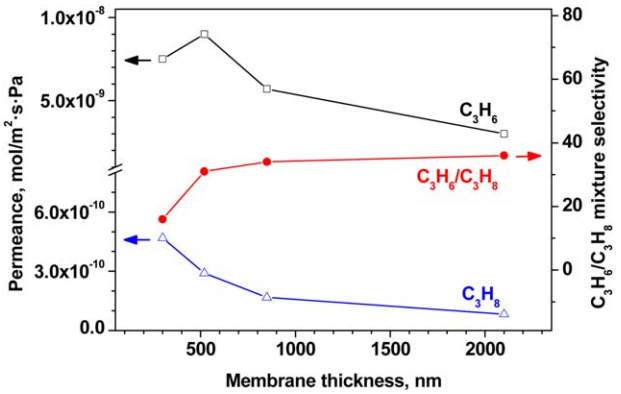

Figure 9. C_3H_6, C_3H_8 gas permeances and C_3H_6/C_3H_8 mixture selectivity of CMS membranes as a function of membrane thickness.

[Color figure can be viewed in the online issue, which is available at wileyonlinelibrary.com.]

a decrease in C_3H_6 permeance and an increase in C_3H_8 permeance. These results suggest that some dramatic pore structure change has taken place when reducing the carbon layer thickness from 520 to 300 nm.

To better interpret the pore structure change associated with the membrane thickness, permeabilities for the four studied gases were calculated from the permeances, and plotted as a function of membrane thickness. As shown in Figure 10, the permeability values for He, N_2, and C_3H_6 decrease with lowering the thickness, with the most significant reduction occurring at 300 nm. However, the C_3H_8 permeability almost keeps unchanged. These thickness dependences of permeabilities, together with the mixture selectivity results shown above indicate that: (1) the membrane experiences a reduction in the porosity with thickness decreasing from 2100 to 520 nm; (2) as thickness is further reduced to 300 nm, the effective pore size of the membrane drastically decreases as well.

The micropores in CMS membranes are formed by the misalignment/imperfect packing of the aromatic domains/carbon sheets.[30,31] The piling of polymer precursor chains on support before pyrolysis has been reported to have influences on the final CMS pore structure.[32,33] Irregularly arrayed polymer chains tend to form bigger CMS pores, while orderly and tightly arranged polymer chains will result in a smaller distance between the carbon sheets. For the polymer membranes prepared in our work, a more closely packed polymer chains in the thinnest polymer film coated on the support has been suggested by the slightly higher He/N_2 perm-selectivity for membrane P-0.2-15 (Figure 3) compared with the others. As discussed above, after this membrane is pyrolyzed, a more restricted pore structure can be expected.

The glass transition temperature T_g, which is directly related to the chain segmental mobility of the polymer, is another key factor influencing polymer-carbon transition during the pyrolysis and the pore structure formation of the final CMS membrane.[31,34] Polymer precursor with higher T_g possesses higher chain rigidity to prevent pore collapses in the intermediate stage during pyrolysis and help the membrane retain the desirable pore structure. Conversely, lower T_g, which implies higher molecular mobility, facilitates the reorganization of carbon chains and leads to a more closely packed carbon sheets. It is well known that for free standing polymer films and supported polymer films on nonattractive substrates, the glass transition temperature for the polymer decreases as the film thickness decreases.[35,36] This film thickness dependence of T_g causes a faster physical aging for a polymer membrane with a smaller thickness. It was recently reported that the thermal rearrangement of an ortho-functional polyimide and the gas transport properties of thermal rearranged (TR) films are also strongly film thickness dependent.[37,38] Thin TR film has a higher degree of chemical conversion, and experiences a much greater rate of physical aging than the thick films. The lower glass transition temperature, the higher segmental chain mobility for the thinner polymer film is believed to be the main reason behind these phenomena.

The physical aging behavior of our γ-alumina supported polymer membranes was measured by tracking the gas permeances and selectivity over time. As shown in Figures 11 and 12, the thinner the membranes, the more rapid the rate for the decrease of normalized He, N_2 permeance, and the higher the normalized He/N_2 perm-selectivity over aging time. This effect is more pronounced for the 386-nm membrane. These results reflect a much higher chain segmental mobility for the 386-nm polymer membrane, which allows the aromatic domains/carbon chains extra freedom to become more closely packed and form smaller micropores in the 300-nm CMS membrane.

In addition, the release of volatile products during pyrolysis might also play some role in the structure change. The thinner film clearly provides a shorter pathway for the diffusion and release of volatile products from the membrane. Wang et al.[38] reported that the reduced diffusional resistance for the evolving volatile compounds is one possible cause for the much larger weight loss and higher degree of chemical conversion observed for a thinner TR membrane. Hatori et al.[21] also found that the thinner the film, the more weight is lost during the pyrolysis of polyimide films. Therefore for the CMS membranes prepared in this work, under the same pyrolysis condition, the thinner film may eventually end up with a higher degree of graphitization and smaller pore size. However, more experiments are required to verify this possible reason.

The combined effects from the packing of polymer chains, chain segmental mobility, and the diffusion of volatile byproducts result in a smaller effective micropore size and

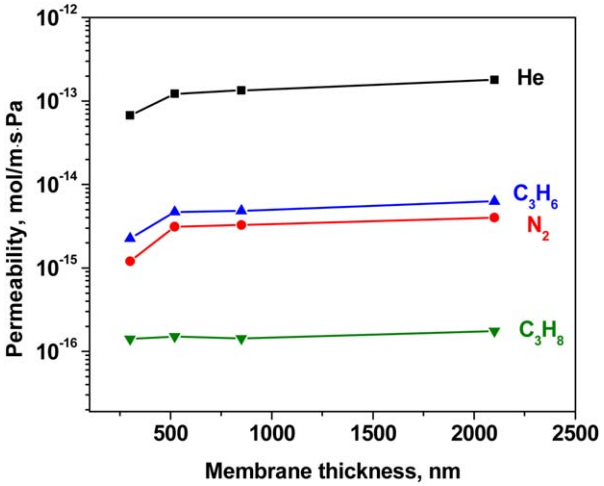

Figure 10. Gas permeabilities of He, N_2, C_3H_6, and C_3H_8 of CMS membranes as a function of membrane thickness.

[Color figure can be viewed in the online issue, which is available at wileyonlinelibrary.com.]

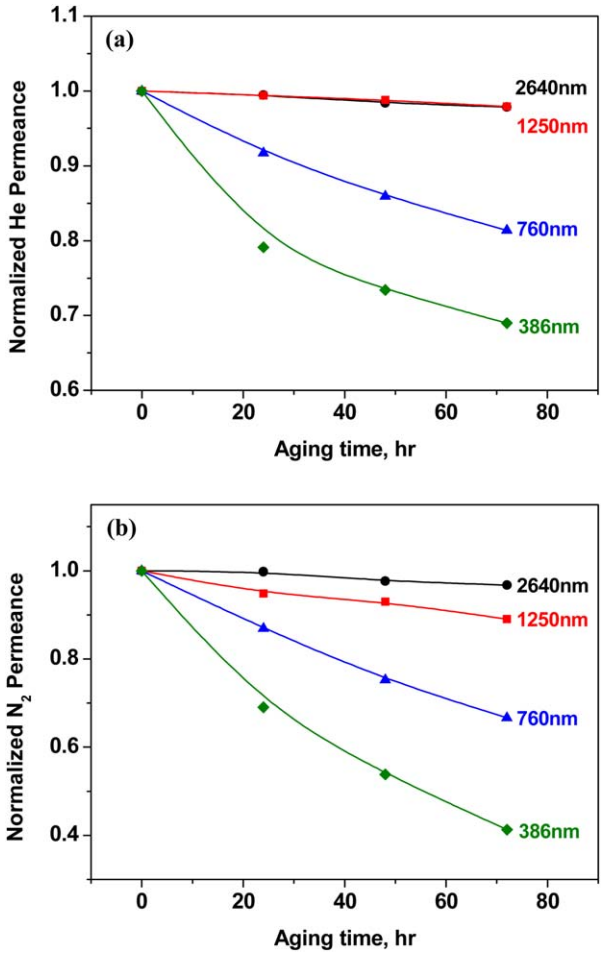

Figure 11. Normalized He (a) and N_2 (b) gas permeances of polymer-alumina compostie membranes with different thickness as a function of aging time.

[Color figure can be viewed in the online issue, which is available at wileyonlinelibrary.com.]

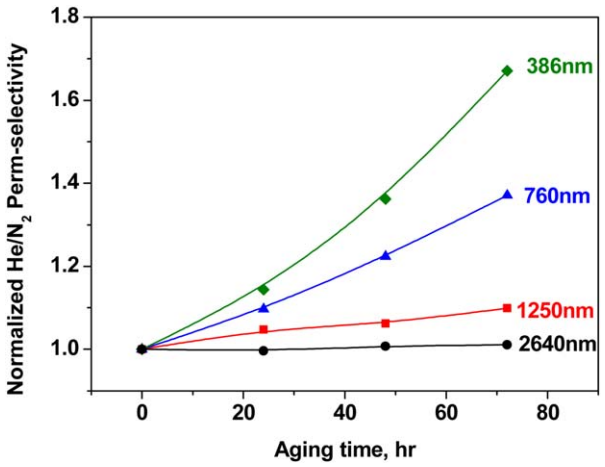

Figure 12. Normalized He/N_2 perm-selectivity of polymer-alumina compostie membranes with different thickness as a function of aging time.

[Color figure can be viewed in the online issue, which is available at wileyonlinelibrary.com.]

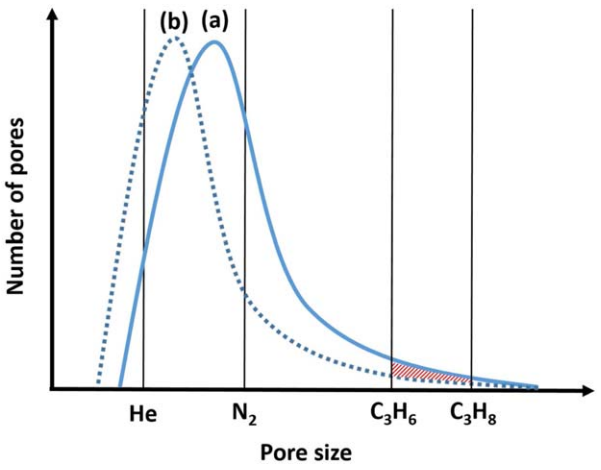

Figure 13. Schematic micropore size distribution for CMS membranes based on the hypothetical qualitative model proposed by Koros and coworkers.[39]

[Color figure can be viewed in the online issue, which is available at wileyonlinelibrary.com.]

smaller amount of these pores for the 300-nm CMS membrane. A hypothetical qualitative micropore size distribution model proposed by Koros was used to explain the unusual gas permeation and separation properties of the 300-nm CMS membrane.[39] Based on Koros's model, the pore-size distributions for the CMS membranes prepared in this work were generated and illustrated in Figure 13. When the membrane thickness was reduced to 300 nm, the distribution curve is very likely to transfer from type (a) to type (b). The four solid straight lines indicate the molecular size of He, N_2, C_3H_6, and C_3H_8. Here we use van der Waals diameter, instead of kinetic diameter, for these four molecules, which is respectively 2.66, 3.13, 4.03, and 4.16 Å for He, N_2, C_3H_6, and C_3H_8, as reported by Koros and coworkers.[40] It should be noted that the CMS has similar adsorption property for He and N_2, and for C_3H_6 and C_3H_8. Thus, the difference in the permeability between He, N_2 and between C_3H_6 and C_3H_8 is due to the difference in diffusivity as a result of different molecular size.

The micropores locating on the right side of the straight lines in Figure 13 represent the corresponding pores accessible for the transport of each gas. The membrane with type (b) distribution is expected to be more selective but less permeable to the He/N_2 gas pair. However, the permeation of the relatively large C_3H_6 and C_3H_8 molecules through the CMS membrane largely depends on the micropores locating on the tail end of the distribution. As illustrated by the red area, the shift from distribution type (a) to type (b) leads to a significant reduction in the total number of micropores accessible for the transport of C_3H_6, which lowers the permeability of C_3H_6 to a large extent, as suggested by the lower C_3H_6 permeance at even reduced membrane thickness. However, pores that are accessible to C_3H_8 are less affected by the aforementioned effects, which gives an almost unchanged C_3H_8 permeability and allows the permeance of C_3H_8 to continue to increase as the membrane thickness decreases.

Performance improvement by optimization of pyrolysis conditions

It was reported that for a given polymer precursor, performing the pyrolysis at a higher temperature for a longer thermal

Table 2. C_3H_6/C_3H_8 Separation Results of CMS Membranes with the Thickness of ~300 nm Prepared at Different Pyrolysis Conditions, Ramping Rate is 4°C min^{-1} for All Membranes

Membranes	Pyrolysis Temperature (°C)	Thermal Soak Time (h)	C_3H_6 Permeance (mol m^{-2} s^{-1} Pa^{-1})	C_3H_6/C_3H_8 Selectivity
M1	550	2	7.5×10^{-9}	16
M2	550	0.5	8.7×10^{-9}	17
M3	500	0.5	1.4×10^{-8}	23

soak time leads to a smaller effective pore size of the pyrolysis-derived CMS membrane, and vice versa.[25,39] To obtain the desirable pore structure of the membrane with carbon layer thickness of less than 500 nm, pyrolysis was performed at lower temperature for a shorter period to minimize reduction in the pore size. As shown in Table 2, as the final pyrolysis temperature lowered to 500°C and the thermal soak time reduced to 0.5 h, membrane M3 shows improved permeance and selectivity, as compared with membrane M1. The improvement is most likely caused by forming a more favorable pore structure with the pore distribution close to type (a) in Figure 13. However, the selectivity is still lower than those of the membranes with selective layer thickness of above 500 nm, suggesting that the pore structure is not completely retained even under the more gentle pyrolysis condition, and tuning of precursor structure is probably necessary for further performance improvement. Nevertheless, this is beyond the scope of this study.

Figure 14 compares the C_3H_6/C_3H_8 mixture selectivity and C_3H_6 permeance (at <50°C) for the CMS membranes prepared in this work with various other membranes reported in literature. The upper-bound trade-off curve for CMS membranes was generated based on reported data, and the curve for polymer membranes was created using the reported permeability and selectivity upper-bound curve[41] assuming the membrane thickness to be around 500 nm. The CMS membranes with the thickness of around 520 nm prepared in this work exhibit a mixture selectivity of around 31, and a C_3H_6 permeance up to 1.0×10^{-8} mol m^{-2} s^{-1} Pa^{-1}. As shown, the performances of the CMS membranes prepared in this work are above the upper-bound curve for the reported CMS membranes and polymer membranes, and close to the performances of ZIF-8- and silica-based membranes.

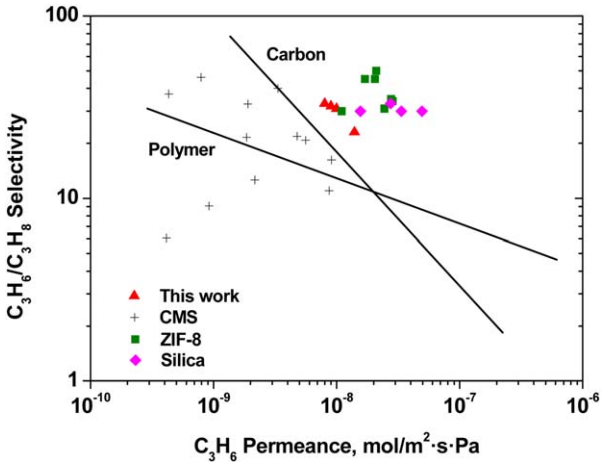

Figure 14. C_3H_6/C_3H_8 mixture selectivity as a function of C_3H_6 permeance (at <50°C) for polymer,[41] CMS,[11–14,18,19,42] ZIF-8,[43–45] and silica[46,47] membranes.

The solid line shows the upper-bound trade-off curve for polymer membranes and CMS membranes reported in the literature to date. [Color figure can be viewed in the online issue, which is available at wileyonlinelibrary.com.]

Membrane cost is an important factor to be considered for practical application. The major share of the cost for the supported CMS membrane comes from the underlying porous substrate. For scaling up, ceramic hollow fibers can be used as the substrates to deliver high membrane packing density comparable with that of free-standing CMS hollow fiber membranes. As demonstrated in our work, coating a γ-alumina intermediate layer can significantly improve the support quality as well as the membrane performance, making it possible to use relatively cheap low quality ceramic hollow fibers as supports to reduce the overall membrane cost. On the other hand, at a similar C_3H_6/C_3H_8 mixture selectivity, for example, ~30, the permeance of alumina supported CMS membrane is around 3–10 times that of other reported CMS membranes, as shown in Figure 14. The greatly improved permeance means smaller membrane area, which could compensate the relatively high cost of ceramic support, making ceramic supported CMS membrane system a cost-effective option for practical application.

Conclusions

Ultrathin, high quality CMS membranes of various thicknesses (300–2100 nm) were synthesized on mesoporous γ-alumina support by pyrolysis of polymer films of different thicknesses. The gas permeation properties and micropore structure of the CMS membranes depend on membrane thickness. With the membrane thickness decreasing from 2100 to 520 nm, the gas permeance of the studied gases He, N_2, C_3H_6, and C_3H_8 increases, and the He/N_2 and C_3H_6/C_3H_8 selectivities almost keep constant with decreasing membrane thickness. However, further reduction in thickness to 300 nm causes an increase in He/N_2 selectivity, but a decrease in C_3H_6/C_3H_8 selectivity. These findings suggest that the 300-nm CMS membrane contains micropores in smaller size and lower quantity as compared with the other membranes with larger thickness. The change in micropore structure might be due to the more close packing of polymer chains, higher chain segmental mobility, and the faster release of volatile products during pyrolysis for the thinner polymer films. The CMS membranes prepared in our work show excellent C_3H_6/C_3H_8 mixture separation performances, especially a high C_3H_6 permeance offered by the ultrathin membrane layer.

Acknowledgments

The authors would like to acknowledge the support of the National Science Foundation (IIP-1127395) for this project, and Belle K. Lin for assistance in some experiments. The authors also acknowledge the use of facilities with the LeRoy Eyring Center for Solid State Science at Arizona State University.

Literature Cited

1. Lin YS, Kumakiri I, Nair BN, Alsyouri H. Microporous inorganic membranes. *Sep Purif Methods*. 2002;31(2):229–379.
2. Ismail AF, David LIB. A review on the latest development of carbon membranes for gas separation. *J Membr Sci*. 2002;193(1):1–18.
3. Anderson M, Wang HB, Lin YS. Inorganic membranes for carbon dioxide and nitrogen separation. *Rev Chem Eng*. 2012;28(2–3):101–121.
4. Salleh WNW, Ismail AF, Matsuura T, Abdullah MS. Precursor selection and process conditions in the preparation of carbon membrane for gas separation: a review. *Sep Purif Rev*. 2011;40(4):261–311.
5. Briceno K, Garcia-Valls R, Montane D. State of the art of carbon molecular sieves supported on tubular ceramics for gas separation applications. *Asia-Pac J Chem Eng*. 2010;5(1):169–178.
6. Saufi SM, Ismail AF. Fabrication of carbon membranes for gas separation—a review. *Carbon*. 2004;42(2):241–259.
7. Barsema JN, Klijnstra SD, Balster JH, van der Vegt NFA, Koops GH, Wessling M. Intermediate polymer to carbon gas separation membranes based on Matrimid PI. *J Membr Sci*. 2004;238(1):93–102.
8. Eldridge RB. Olefin paraffin separation technology—a review. *Ind Eng Chem Res*. 1993;32(10):2208–2212.
9. Motelica A, Bruinsma OSL, Kreiter R, den Exter M, Vente JF. Membrane retrofit option for paraffin/olefin separation—a technoeconomic evaluation. *Ind Eng Chem Res*. 2012;51(19):6977–6986.
10. Faiz R, Li K. Polymeric membranes for light olefin/paraffin separation. *Desalination*. 2012;287:82–97.
11. Chng ML, Xiao YC, Chung TS, Toriida M, Tamai S. Enhanced propylene/propane separation by carbonaceous membrane derived from poly (aryl ether ketone)/2,6-bis(4-azidobenzylidene)-4-methyl-cyclohexanone interpenetrating network. *Carbon*. 2009;47(7):1857–1866.
12. Okamoto K, Kawamura S, Yoshino M, Kita H, Hirayama Y, Tanihara N, Kusuki Y. Olefin/paraffin separation through carbonized membranes derived from an asymmetric polyimide hollow fiber membrane. *Ind Eng Chem Res*. 1999;38(11):4424–4432.
13. Xu LR, Rungta M, Koros WJ. Matrimid (R) derived carbon molecular sieve hollow fiber membranes for ethylene/ethane separation. *J Membr Sci*. 2011;380(1):138–147.
14. Bhuwania N, Labreche Y, Achoundong CSK, Baltazar J, Burgess SK, Karwa S, Xu LR, Henderson CL, Williams PJ, Koros WJ. Engineering substructure morphology of asymmetric carbon molecular sieve hollow fiber membranes. *Carbon*. 2014;76:417–434.
15. Merkel TC, Lin HQ, Wei XT, Baker R. Power plant post-combustion carbon dioxide capture: an opportunity for membranes. *J Membr Sci*. 2010;359(1):126–139.
16. Hayashi JI, Mizuta H, Yamamoto M, Kusakabe K, Morooka S. Pore size control of carbonized BPDA-pp′ODA polyimide membrane by chemical vapor deposition of carbon. *J Membr Sci*. 1997;124(2):243–251.
17. Lee HJ, Kim DP, Suda H, Haraya K. Gas permeation properties for the post-oxidized polyphenylene oxide (PPO) derived carbon membranes: effect of the oxidation temperature. *J Membr Sci*. 2006; 282(1–2):82–88.
18. Hayashi J, Mizuta H, Yamamoto M, Kusakabe K, Morooka S, Suh SH. Separation of ethane/ethylene and propane/propylene systems with a carbonized BPDA-pp′ODA polyimide membrane. *Ind Eng Chem Res*. 1996;35(11):4176–4181.
19. Yamamoto M, Kusakabe K, Hayashi J, Morooka S. Carbon molecular sieve membrane formed by oxidative carbonization of a copolyimide film coated on a porous support tube. *J Membr Sci*. 1997; 133(2):195–205.
20. Hatori H, Yamada Y, Shiraishi M. In-plane orientation and graphitizability of polyimide films: II. Film thickness dependence. *Carbon*. 1993;31(8):1307–1312.
21. Hatori H, Yamada Y, Shiraishi M, Yoshihara M, Kimura T. The mechanism of polyimide pyrolysis in the early stage. *Carbon*. 1996; 34(2):201–208.
22. Ma XL, Lin BK, Wei XT, Kniep J, Lin YS. Gamma-alumina supported carbon molecular sieve membrane for propylene/propane separation. *Ind Eng Chem Res*. 2013;52(11):4297–4305.
23. Chang CH, Gopalan R, Lin YS. A comparative study on thermal and hydrothermal stability of alumina, titania and zirconia membranes. *J Membr Sci*. 1994;91(1):27–45.
24. Cooper CA, Lin YS. Microstructural and gas separation properties of CVD modified mesoporous γ-alumina membranes. *J Membr Sci*. 2002;195(1):35–50.
25. Geiszler VC, Koros WJ. Effects of polyimide pyrolysis conditions on carbon molecular sieve membrane properties. *Ind Eng Chem Res*. 1996;35(9):2999–3003.
26. Kiyono M, Williams PJ, Koros WJ. Generalization of effect of oxygen exposure on formation and performance of carbon molecular sieve membranes. *Carbon*. 2010;48(15):4442–4449.
27. Lagorsse S, Magalhaes FD, Mendes A. Aging study of carbon molecular sieve membranes. *J Membr Sci*. 2008;310(1):494–502.
28. Zhao ZX, Ma XL, Li Z, Lin YS. Synthesis, characterization and gas transport properties of MOF-5 membranes. *J Membr Sci*. 2011; 382(1):82–90.
29. Zhao ZX, Ma XL, Kasik A, Li Z, Lin YS. Gas separation properties of metal organic framework (MOF-5) membranes. *Ind Eng Chem Res*. 2013;52(3):102–1108.
30. Shiflett MB, Foley HC. On the preparation of supported nanoporous carbon membranes. *J Membr Sci*. 2000;179(1):275–282.
31. Shao L, Chung TS, Pramoda KP. The evolution of physicochemical and transport properties of 6FDA-durene toward carbon membranes; from polymer, intermediate to carbon. *Microporous Mesoporous Mater*. 2005;84(1):59–68.
32. Tseng HH, Shih KM, Shiu PT, Wey MY. Influence of support structure on the permeation behavior of polyetherimide-derived carbon molecular sieve composite membrane. *J Membr Sci*. 2012;405:250–260.
33. Wey MY, Tseng HH, Chiang CK. Improving the mechanical strength and gas separation performance of CMS membranes by simply sintering treatment of α-Al_2O_3 support. *J Membr Sci*. 2014;453: 603–613.
34. Tin PS, Chung TS, Hill AJ. Advanced fabrication of carbon molecular sieve membranes by nonsolvent pretreatment of precursor polymers. *Ind Eng Chem Res*. 2004;43(20):6476–6483.
35. Huang Y, Paul DR. Physical aging of thin glassy polymer films monitored by gas permeability. *Polymer*. 2004;45(25):8377–8393.
36. Rowe BW, Freeman BD, Paul DR. Physical aging of ultrathin glassy polymer films tracked by gas permeability. *Polymer*. 2009;50(23): 5565–5575.
37. Wang H, Chung TS, Paul DR. Physical aging and plasticization of thick and thin films of the thermally rearranged ortho-functional polyimide 6FDA-HAB. *J Membr Sci*. 2014;458:27–35.
38. Wang H, Chung TS, Paul DR. Thickness dependent thermal rearrangement of an ortho-functional polyimide. *J Membr Sci*. 2014;450: 308–312.
39. Steel KM, Koros WJ. An investigation of the effects of pyrolysis parameters on gas separation properties of carbon materials. *Carbon*. 2005;43(9):1843–1856.
40. Zhang C, Lively RP, Zhang K, Johnson JR, Karvan O, Koros WJ. Unexpected molecular sieving properties of zeolitic imidazolate framework-8. *J Phys Chem Lett*. 2012;3(16):2130–2134.
41. Burns RL, Koros WJ. Defining the challenges for C_3H_6/C_3H_8 separation using polymeric membranes. *J Membr Sci*. 2003;211(2):299–309.
42. Xu LR, Rungta M, Brayden MK, Martinez MV, Stears BA, Barbay GA, Koros WJ. Olefins-selective asymmetric carbon molecular sieve hollow fiber membranes for hybrid membrane-distillation processes for olefin/paraffin separations. *J Membr Sci*. 2012;423:314–323.
43. Pan YC, Li T, Lestari G, Lai ZP. Effective separation of propylene/propane binary mixtures by ZIF-8 membranes. *J Membr Sci*. 2012; 390:93–98.
44. Liu DF, Ma XL, Xi HX, Lin YS. Gas transport properties and propylene/propane separation characteristics of ZIF-8 membranes. *J Membr Sci*. 2014;451:85–93.
45. Kwon HK, Jeong HK. In situ synthesis of thin zeolitc-imidazolate framework ZIF-8 membranes exhibiting exceptionally high propylene/propane separation. *J Am Chem Soc*. 2013;135(29):10763–10768.
46. Kanezashi M, Shazwani WN, Yoshioka T, Tsuru T. Separation of propylene/propane binary mixtures by bis(triethoxysilyl) methane (BTESM)-derived silica membranes fabricated at different calcination temperatures. *J Membr Sci*. 2012;415:478–485.
47. Kanezashi M, Miyauchi S, Nagasawa H, Yoshioka T, Tsuru T. Gas permeation properties through Al-doped organosilica membranes with controlled network size. *J Membr Sci*. 2014;466:246–252.

Manuscript received Apr. 6, 2015, and revision received July 7, 2015.